Temperature Mapping of Stacked Silicon Dies from X-Ray-Diffraction Intensities

Darshan Chalise,[1,2,*] Peter Kenesei,[3] Sarvjit D. Shastri,[3] and David G. Cahill[1,2,4,†]

[1] *Department of Physics, University of Illinois at Urbana-Champaign, Urbana, Illinois 61801, USA*
[2] *Materials Research Laboratory, University of Illinois at Urbana-Champaign, Urbana, Illinois 61801, USA*
[3] *X-ray Science Division, Argonne National Laboratory, Lemont, Illinois 60439, USA*
[4] *Materials Science and Engineering, University of Illinois at Urbana-Champaign, Urbana, Illinois 61801, USA*

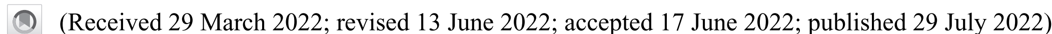
(Received 29 March 2022; revised 13 June 2022; accepted 17 June 2022; published 29 July 2022)

Increasing power densities in integrated circuits have led to an increased prevalence of thermal hotspots in integrated circuits. Tracking these thermal hotspots is imperative to prevent circuit failures. In three-dimensional (3D) integrated circuits, conventional surface techniques like infrared thermometry are unable to measure the 3D temperature distribution, and optical and magnetic resonance techniques are difficult to apply due to the presence of metals and large current densities. X-rays offer a high penetration depth and can be used to probe 3D structures. We report a method utilizing the temperature dependence of x-ray-diffraction intensity via the Debye-Waller factor to simultaneously map the temperature of individual silicon dies in a stack. Utilizing beamline 1-ID-E at the Advanced Photon Source (Argonne), we demonstrate, for each individual silicon die, a temperature resolution of 3 K, a spatial resolution of $100 \times 400\ \mu\text{m}^2$, and a temporal resolution of 20 s. Utilizing a sufficiently high-intensity laboratory source, e.g., from a liquid-anode source, this method can be scaled down to laboratories for noninvasive temperature mapping of 3D integrated circuits.

DOI: 10.1103/PhysRevApplied.18.014076

I. INTRODUCTION

The increase in power density of processors has led to an increase in the occurrence of thermal hot spots within the processors [1,2]. The locations of the thermal spots change with time, and therefore, tracking them is difficult. Tracking of the hot spots, however, is important, as most failure mechanisms in the processors have a strong temperature dependence [1].

Traditionally, the processor dies are embedded with thermal sensors to measure the temperature during operation [1]. However, these sensors provide only single-point temperature measurements and cannot provide full-field temperature information. Contact-based thermometry techniques like scanning thermal microscopy [3] cannot be used to probe three-dimensional (3D) integrated circuits (ICs), as probing layers underneath the top die would compromise the structural integrity of the device. Therefore, a noncontact full-field thermometry technique is required to map the temperature in 3D ICs.

Infrared thermometry can be used to measure the temperature distribution of the surface of a single die [2]. In 3D ICs, there are several interfaces that scatter the infrared radiation due to the difference in refractive indices of the media [4]. Without precise knowledge of the location of the interfaces and the optical properties of the media, the interpretation of observed radiation that is emitted from the surface of the sample to recover 3D temperature information is impossible. Furthermore, silicon is only transparent in the infrared range of wavelength 1.2–15 μm [5,6], and therefore, detecting infrared radiation from inner dies to reconstruct the temperature field is impractical. Optical techniques like thermoreflectance imaging [7] or optical coherence tomography [8] would also be impractical due to the strong absorption of visible or near-infrared light by a metal-silicon composite, even with a small amount of metal [9,10].

High-energy x-rays have a great penetration depth for most materials [11], and therefore, offer the possibility for noninvasively probing structures like stacked silicon dies. For example, a 30-keV x-ray beam has a penetration depth of 100 μm in copper and 3 mm in silicon [11], and therefore, it could be used to probe about 10 layers (normal incidence) of a composite structure with 10-μm copper and 100-μm silicon. At 70 keV (approximate energy used in the current experiment), the penetration depth increases to 1 mm in copper and 2 cm in silicon [11], and significantly thicker samples can be probed.

In general, several features of x-ray diffraction depend on temperature. X-ray peaks shift due to changes in the lattice parameter, the structure factor changes due to

*darshan2@illinois.edu
†d-cahill@illinois.edu

 © 2022 American Physical Society

thermally excited lattice vibration (Debye-Waller factor), and peaks can broaden due to inhomogeneous strain induced by differences in the thermal expansion of adjoining materials [12,13]. Therefore, the measurement of x-ray intensity provides a means of noninvasive thermometry of stacked structures like 3D integrated circuits.

Sensitivity analysis can be used to determine which x-ray method has the highest temperature dependence. The sensitivity coefficient, given by $\xi_T = (\partial \ln S/\partial \ln T)$, measures the percentage change in signal, S, with respect to 1% change in temperature, T [14,15]. In measuring the change in the lattice parameter due to temperature, the lattice parameter changes by about 6×10^{-6} rad for 1% (3 K) change in temperature. Therefore, measurements with a temperature resolution of 1 K would require the resolution of a Bragg center of about 2 μrad. The sensitivity coefficient of the measurement of thermally induced strain is similar because of the small coefficients of thermal expansion of materials, which are about $2 - 3 \times 10^{-6}\mathrm{K}^{-1}$ [11,16].

The measurement of the Debye-Waller factor via the reduction of diffraction intensity can provide a much better sensitivity in temperature measurements compared to changes in the Bragg center [17,18] [As discussed below, we predict and observe $\xi_T \sim 2.5$ for the measurement of the (16 0 0) diffraction peak of silicon.] Therefore, this experiment proposes a method for measuring the relative change in the Debye-Waller factor to measure the temperature of different layers of stacked silicon dies. The experiment utilizes rastering of an x-ray beam across the sample to produce a map of diffraction intensities, and thereby, of temperature. Simultaneous mapping of different dies in a stack is possible due to the spatial separation of beams that are diffracted from different dies in the stack.

II. THEORY

Thermal vibrations modify the structure factor (scattering amplitude) of the unit cell, which can be described by the introduction of a temperature factor, e^{-M} [19], i.e.,

$$|F_{\mathrm{mod}}| = |F|e^{-M},$$

where $M = (2\pi(\mathbf{s})^2\Delta X^2)/3$; ΔX^2 is the average quadratic displacement of an atom from its mean position, and $\mathbf{s}$ is the scattering vector. $\mathbf{s} = (2 \sin \theta)/\lambda$ in the case of the Bragg reflection, with θ as the Bragg angle and λ as the incident wavelength.

M can be calculated approximately within the Debye model [20]:

$$M = \frac{6h^2T\left[\psi(\tau) + \frac{\chi}{4}\right]\left(\frac{\sin\theta}{\lambda}\right)^2}{mkT_D}.$$

Here, h is the Planck constant, T is the temperature of the measured region, m is the mass of the silicon atom, k is the Boltzmann constant, θ is the Bragg angle, and λ is the x-ray wavelength. θ_M is the average Debye temperature given by $3/T_D^2 = 1/T_{D,l}^2 + 2/T_{D,t}^2$, where $T_{D,l}$ and $T_{D,t}$ are Debye temperatures for the longitudinal and transverse modes of lattice vibrations, respectively. For silicon, $T_D = 543$ K [21]. $[\psi(\tau) + (\tau/4)]$ is the Debye function, where $\tau = (T_D/T)$. The value of the Debye function is close to unity for the temperature range $T > (T_D/2)$ and is given by $[\psi(\tau) + (\tau/4)] \approx 1 + (\tau^2/36) - (\tau^4/3600)$ [12].

At room temperature, the mean square atomic displacement, ΔX^2, estimated by the Debye model is 0.0058 Å^2, and this compares extremely well with ΔX^2 calculated from the dispersion of Si using inelastic neutron scattering (0.0059 Å^2) [17], and therefore, the Debye model can be reliably used to predict the temperature dependence of the structure factor.

For most materials, the integrated intensity of diffraction is directly proportional to the square of the structure factor, $|F|^2$. This is according to kinematic theory, which states that the diffraction intensities from each small-volume elements of a crystal add incoherently, and the effects of multiple reflection of the same beam within the crystal need not be considered [4,19]. Multiple reflections can be neglected for most crystals, as imperfections resulting from lattice faults do not allow the Bragg condition to be met for the reflected beam [19]. Kinematic diffraction results in a decrease in integrated intensity by the temperature factor, e^{-2M}, known as the Debye-Waller factor [12].

Silicon, however, can be free from defects or dislocations for large length scales [4]. Therefore, high-quality silicon can be considered a nearly perfect crystal, for which the reflected beams also satisfy the Bragg condition. The diffraction in silicon may require an explanation using the dynamic theory of diffraction, which takes into account the effect of multiple scattering. The integrated intensity in a dynamic diffraction is proportional to the amplitude of the structure factor, and not the square of the structure factor as in the case of kinematic diffraction [12].

Batterman suggested two ways of interpreting the effect of thermal vibration in the case of dynamic diffraction [20]. The first is that multiple scattering still takes place in the case of thermal vibrations, but the decrease in scattering amplitude due to the decrease in the structure factor results in x-rays seeing more atoms and in narrowing of the condition (Darwin width) for perfect refection (combined amplitude reflectivity approaching 1). The second way to interpret the effect of thermal vibration is that it degrades the perfection of the crystal, which would result in kinematic diffraction from the crystal [20]. Using beams with a bandwidth smaller than the expected Darwin widths, for (444), (555), and (660) reflections in thick and nearly perfect silicon crystal (impurities $\leq 10^{15}/\mathrm{cm}^3$), Batterman observed dynamic diffraction with peak narrowing that scaled linearly with the decrease in the structure factor,

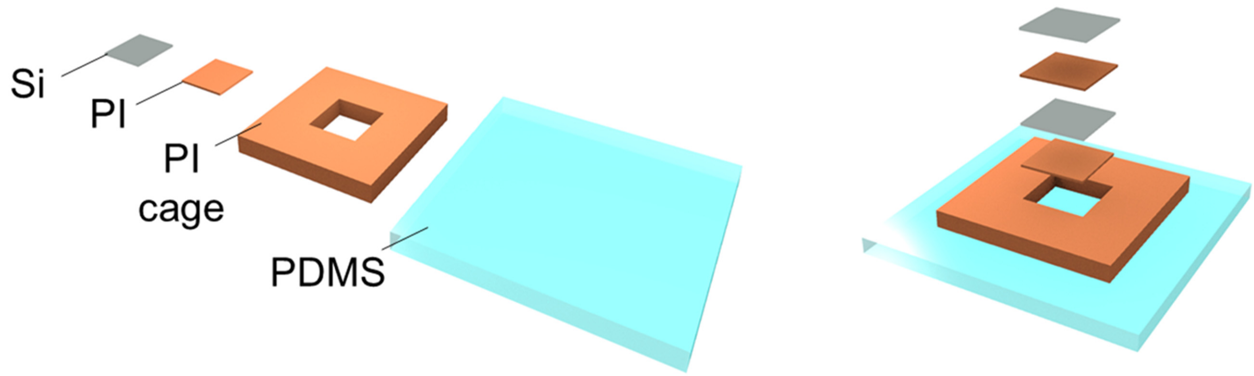

FIG. 1. Schematic of the stacking of two silicon dies. Stacking is performed on top of a polydimethylsiloxane (PDMS) layer using a polyimide cage. 125-μm polyimide layer separates the two silicon dies. The silicon and the polyimide layers are 1 cm × 1 cm in area.

with no change in height of the rocking curve [21]. This results in a decrease in the intensity (integrated over the rocking curve) proportional to the decrease in the structure factor, i.e., the integrated intensity decreases by a factor of e^{-M}. Kohra *et al.* also observed an e^{-M} dependence of the integrated intensity for dynamic diffraction from nearly perfect silicon and germanium crystals [22,23].

To hypothesize if we expect dynamic diffraction in our experiment, one important parameter to look at is the x-ray extinction length. The extinction length is the path length through the crystal for which the amplitude reflectivity of the x-rays approaches 1 and is given by $\Lambda_{\text{ext}} = (1 v_c / 4 d r_0 |F|)$, where d is the plane spacing, r_0 is the Thompson scattering length, and v_c is the volume of the primitive unit cell [4]. For the current experimental conditions, for perfect silicon, the extinction lengths for (8 0 0), (12 0 0), and (16 0 0) are 15 μm (sigma polarization), 51 μm (sigma polarization), and 143 μm, respectively [24]. These lengths are smaller than the x-ray path length in a single die in our experiment (192 μm, 128 μm, and 400 μm, respectively). Therefore, for a perfect silicon crystal, under the experimental conditions used (Sec. III), we expect dynamic diffraction.

Silicon used in the experiment, however, is grown by the Czochralski (CZ) method, which has an oxide concentration of 10^{17}–10^{18} cm^{-3} [25]; this is 2–3 orders of magnitude larger than the impurity concentration in nearly perfect silicon used by Kohra *et al.* and Batterman. In transmission-diffraction geometry, CZ-grown silicon has shown significant deviation from dynamic theory, as dynamic diffraction is extremely susceptible to impurity-induced strain [25]. For the high-momentum transfers investigated in the experiment, impurity-induced strains are expected to have an even more significant effect, as the per plane reflectivity is small and the extinction depths are large. Therefore, we could have results where diffraction significantly deviates from dynamic theory and approaches the kinematic limit. The temperature dependence of the diffraction intensities should elucidate if the diffraction is kinematic or dynamic, as kinematic diffraction has a

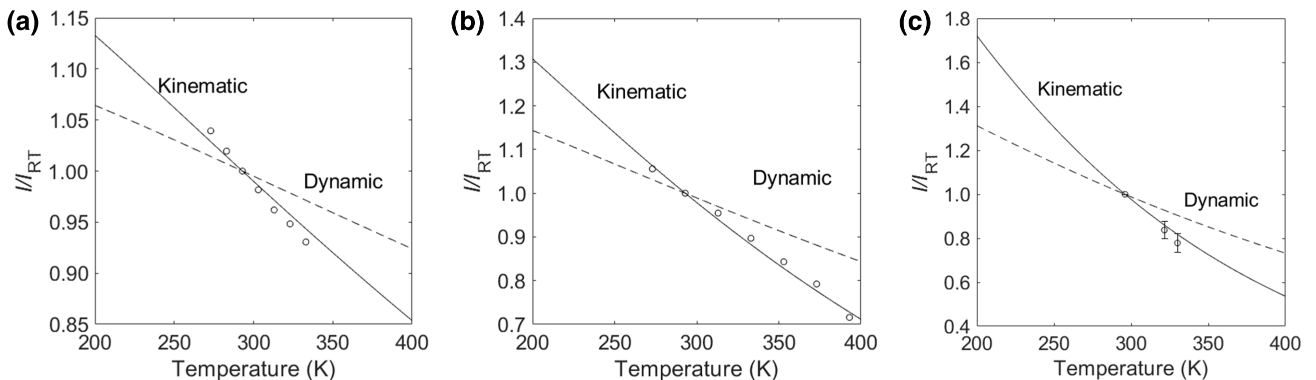

FIG. 2. Temperature dependence of diffraction intensities for (a) (8 0 0), (b) (12 0 0), and (c) (16 0 0) planes. (8 0 0) and (12 0 0) are measured using a Bruker D8 instrument using Mo $K\alpha$ radiation, while (16 0 0) is measured using 72-keV synchrotron radiation at beamline 1-ID-E at the Advanced Photon Source. Diffraction intensities are normalized with the intensity at 293 K for (8 0 0) and (12 0 0) planes and at 296 K for the (16 0 0) plane. Error bars for Fig 2(c) are calculated from measurements taken at five different spots in a die. Temperature dependence for each reflection is consistent with the expectation from kinematic theory of diffraction.

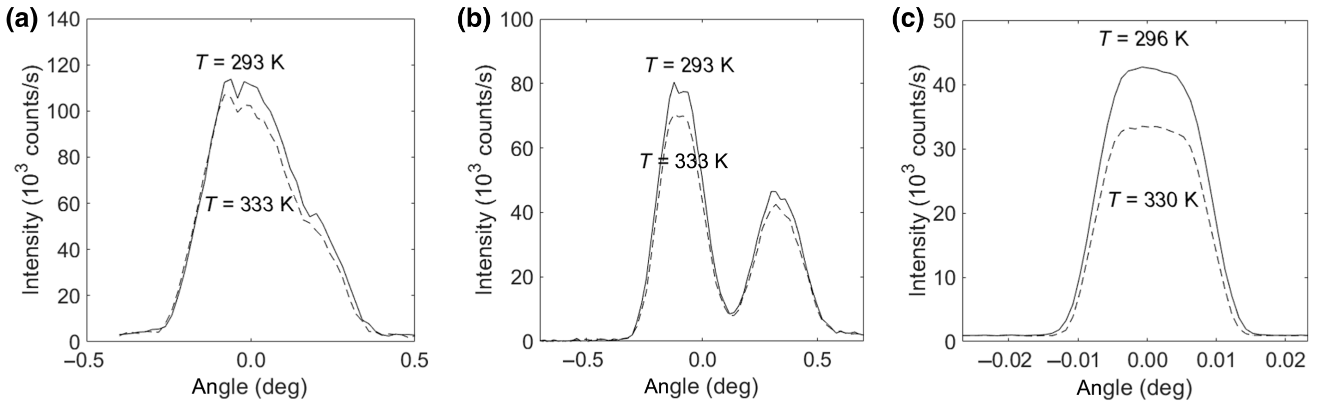

FIG. 3. Rocking curves for (a) (8 0 0) and (12 0 0) planes at $T = 293$ K and $T = 333$ K, and (c) (16 0 0) plane at $T = 296$ K and $T = 330$ K. Rocking curves (a) and (b) are obtained using Mo $K\alpha$ beam, while (c) uses 72-keV synchrotron source. Angles indicate rocking angles around the Bragg maximum. (12 0 0) plane shows two distinct Mo $K\alpha_1$ and Mo $K\alpha_2$ peaks, while the two peaks are not well resolved for the (8 0 0) plane. Decrease in width of the rocking curve is negligible compared to the decrease in peak intensity.

temperature dependence of e^{-2M}, while dynamic diffraction has a temperature dependence of e^{-M}.

III. EXPERIMENTAL DETAILS

CZ-grown undoped (1 0 0) silicon dies ($\rho > 400\ \Omega$ cm) with a thickness of 100 μm and area of 10×10 mm^2 are obtained from UniversityWafer Inc. The stacking of two dies (Fig. 1) is performed using a polyimide (PI) cage with a layer of 125-μm polyimide separating the two dies. The 125-μm polyimide used for stacking is purchased from Sigma Aldrich (GF74134380) and is laser cut to obtain the cage and the separator.

The temperature dependence of (8 0 0) and (12 0 0) diffractions (symmetric Bragg geometry) is measured on a single 100-μm silicon die on a Bruker D8 Advance diffractometer at the School of Chemical Science at the University of Illinois. Temperature is controlled using an Oxford Instruments M8 temperature controller. Mo $K\alpha$ radiation ($E = 17.45$ keV), monochromatized with Gobel-type graded multilayer mirrors [26] to get an energy resolution of $\Delta E/E \approx 5 \times 10^{-2}$ and a beam divergence of about 5 mrad, is incident on the sample with a flux of about 10^7 photons/s and a beam cross section of about $180 \times 180\ \mu$m^2. Diffraction intensities are measured on a Bruker Photon II detector, and the diffraction rocking curves for (8 0 0) and (12 0 0) are recorded with a 4° sweep around the Bragg peak with steps of 0.01°. Integration times of 4 s and 2 s, respectively, are used for each step. Detector files (.sfrm) are read using the FabIO [27] library in PYTHON.

The measurement of the temperature dependence of a (16 0 0) diffraction and mapping of the (16 0 0) diffraction intensities are carried out at beamline 1-ID-E of the Advanced Photon Source, Argonne National Laboratory. Using a bent Si (1 1 1) double-Laue monochromator [28], the beam energy is selected as 72 keV, with a bandwidth ($\Delta E/E$) of 1.3×10^{-3} and a beam divergence of about 1.5 μrad. The wide bandwidth is chosen to relax the stacking accuracy required to meet the Bragg condition simultaneously for the two dies.

A flux of 5×10^9 photons/s is incident on an area of about $400 \times 100\ \mu$m^2 on the sample, resulting in a spatial resolution of $400 \times 100\ \mu$m^2. The sample heating due to this photon flux is negligible (see Sec. I of the Supplemental Material [29]), allowing the diffraction intensity to probe the actual temperature of the sample. Diffraction intensities from the (16 0 0) plane are collected by a Pixirad-1 Cd-Te detector placed in symmetric Bragg geometry ($2\theta = 29.5°$). The separation of the diffracted beams (~175 μm) being larger than Pixirad's pixel separation (60 μm) allows identification of the diffraction peaks from different dies.

The integrated intensity (sum of individual intensities at each point in a Bragg rocking curve) of the (16 0 0) reflection is collected from 121 points of the stacked die sample at room temperature. The sample is rotated by 0.05° around the Bragg angle, with intensities recorded at each $5 \times 10^{-3\circ}$ rotation with an integration time of 2 s per rotation. This results in the measurement time of one spot being 20 s.

Temperature-controlled measurements for the (16 0 0) plane are taken at 296 K, 321 K, and 330 K from five different points of a single silicon die. The die is attached to the hot side of a Peltier cooler, the cold side of which is attached to a heat sink. The Peltier cooler is run at two different voltages to achieve equilibrium temperatures of 321 and 330 K. A thermocouple attached to the surface

of the Peltier module records the temperatures during the measurement.

For measurements using the laboratory x-ray source, i.e., for the (8 0 0) and (12 0 0) planes, the temperature-dependent measurements are repeatable upon heating and cooling. For the (16 0 0) plane, repeatability is not tested due to limited synchrotron time.

IV. RESULTS

Figure 2 shows the temperature dependence of integrated diffraction intensities for the (8 0 0), (12 0 0), and (16 0 0) reflections, and Fig. 3 compares the rocking curves at room temperature to those at 333 K [330 K for the (16 288 0 0) reflection]. The temperature dependence for all the diffractions follows the temperature dependence expected from kinematic theory.

The kinematic diffraction deduced from the temperature dependence contrasts with the dynamic diffraction observed by Batterman and Kohra *et al.* for nearly perfect silicon crystals. The result, however, is not surprising given that CZ-grown Si has a significantly higher impurity concentration that that used by Batterman and Kohra *et al*.

Since the diffractions for all the investigated planes are kinematic, the sensitivity of the diffraction intensity to temperature is double that of the dynamic diffraction. For the (16 0 0) plane, the sensitivity is about 2.5, while for the (12 0 0) plane, the sensitivity is almost halved ($\sim$1.4) and is reduced by a factor of 4 ($\sim$0.65) for the (8 0 0) plane. Therefore, sensitive thermometry using this method would require measuring symmetric Bragg reflections from a high-momentum transfer plane similar to that of the (16 0 0) plane.

An important demonstration using the synchrotron source is to show that the concurrent measurement and separation of diffraction intensities from different layers of stacked dies is possible, given that the pixel size of the detector is smaller than the separation of the reflected beams. In the current experiment, the separation of the beam is given by $x_s = (2s\ \cot\ \theta - H\ \sin\ \theta)\cos\ \theta\ \ (\tan\ (2\theta) - \tan(\theta))$, where s is the distance between the two dies, θ is the Bragg angle, and $H\ \sin\ \theta$ is the spot size of a beam with a $H \times V$ cross section on the sample (details of this calculations are included in Sec. II of the Supplemental Material [29]). For a Bragg angle of about 15° and the separation of dies of about 125 μm, the expected beam separation is about 175 μm along the x axis of the detector (along the axis where the beam is elongated due to the small Bragg angle at incidence).

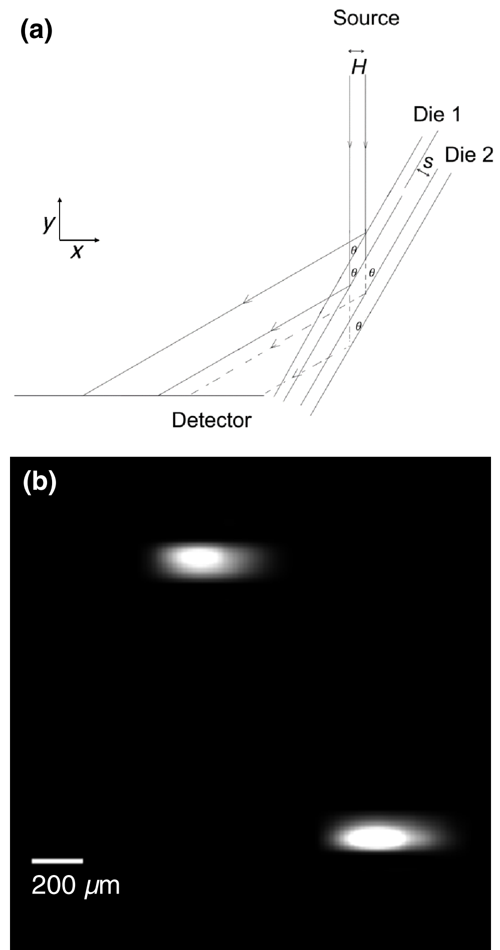

FIG. 4. (a) Schematic of the experimental geometry used in beamline 1-ID-E. x-Axis separation of the beam from top and bottom dies on the detector is a function of the physical separation of the two dies, s, and the Bragg angle, θ, and is given by $x_s = (2s\ \cot\ \theta - H\ \sin\ \theta)\cos\ \theta(\tan\ (2\theta) - \tan(\theta))$. In the present experiment, expected separation along the x axis is about 175 μm. (b) Pixirad image shows Bragg peaks from two dies simultaneously. Spot from the bottom die (top left-hand corner) is less bright (about a factor of $\sim$0.9) than that from the top die. This difference in intensity is expected due to absorption from the top silicon die ($\sim$7%) and the polyimide separator ($\sim$2%). Pixirad image is consistent with the expected about 175-μm separation along the x axis. Separation along the y axis ($\sim$600 μm) is due to the imperfection in the azimuthal (χ) alignment of the dies (estimated to be $\sim$0.6 mrad, as the detector is $\sim$1 m away from the sample) and depends on the sample-to-detector distance.

Figure 4(b) shows a Pixirad image demonstrating that the simultaneous observation of (16 0 0) reflections from two different dies is possible. The top and bottom dies are identified due to the difference in their relative intensities due to x-ray absorption. Separation along the x axis of the detector is similar to the expected value of about 175 μm. The wide bandwidth used in the experiment allows the observation of two different reflections in the same frame. The observation of reflections from different dies in the same frame is, however, not a general requirement, as a complete rocking curve should record diffraction intensities from each die, even if they do not occur in the same frame.

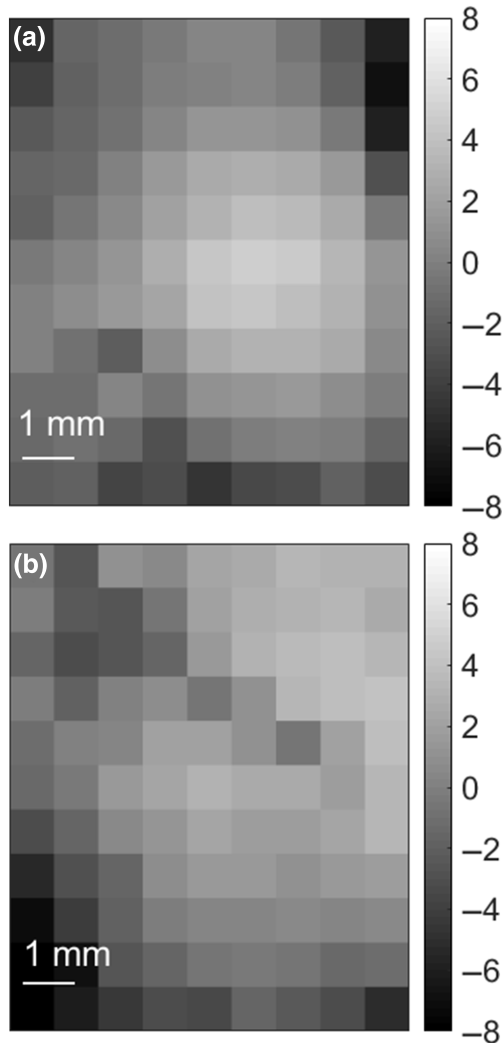

FIG. 5. Distribution of the integrated intensity from 99 spots of (a) die 1 and (b) die 2 at room temperature. Grayscale represents the percentage deviation from the mean value of integrated intensity, with black corresponding to −8% deviation and white corresponding to +8% deviation. Left and right ends of the die are not included in the map as the combined spot size and path length (∼800 μm) is larger than the distance from the edge of the die to the center of the beam (0.5 mm). Rms deviations in intensity at constant temperature is 2.5% and 3%, respectively, for die 1 and die 2. This contributes to temperature uncertainties of 3 and 3.5 K, respectively.

Figures 5(a) and 5(b) show the distribution of integrated intensity at room temperature for the first and second dies in a stack. The rms deviation of the integrated intensity for different points of the sample is about 2.5% for the first die and 2.9% for the second die. Since the diffraction is kinematic, the sensitivity of the diffraction intensity to temperature is about 2.5, and a 2.5% variation in intensity corresponds to a temperature uncertainty of about 3 K.

V. DISCUSSION AND CONCLUSION

Our results show that the simultaneous temperature mapping of different silicon dies in a stack is possible. We demonstrate a mapping technique with a temperature resolution of 3 K, spatial resolution of 400 × 100 μm^2 (the spot size of the beam), and a time resolution of 20 s per spot.

Since the method compares integrated intensities rather than peak intensities for measuring the temperatures of different spots, the method does not suffer from broadening artifacts due to thermal or other mechanical strains, as long as enough points on a rocking curve are recorded [12].

In the case of 3D integrated circuits, the absorption of x-rays due to the presence of metals or circuit components would affect the diffraction intensity from the silicon dies. In that case, a baseline diffraction map at room temperature would be required. A baseline image would also correct for external contamination of the sample, if the sample were not contaminated exactly during the temperature measurement. Even if the sample is contaminated during the measurement, contamination does not affect the diffraction intensity from the samples, as long as the contamination is not thick enough to significantly absorb the incident or diffracted x-rays.

Temperature resolution along the z direction (along the stacking direction) is limited to the x-ray beam path along a particular die. The method requires the separation of the dies to obtain a separability of the Bragg reflections from different dies. The method also requires stacks of single crystals like silicon, which give a single diffraction spot, and requires the orientation of different layers of the single crystal to be close enough so that the rocking curves from all the dies can be recorded in a single θ sweep around a Bragg peak.

In establishing the thermometry technique, we also investigate the nature of diffraction in CZ-grown silicon. We observe that for high-momentum transfer planes in an undoped silicon crystal grown by the CZ method, the diffraction in Bragg geometry, and consequently the temperature dependence of diffraction, is described well by kinematic theory. Given the impurity (non-Si) concentration in CZ silicon is similar for highly doped silicon (regardless of the method of growth), we expect that kinematic theory applies in n-type dies irrespective of the method of their growth.

The spatial resolution of this method can be improved either by using a beam with a smaller cross section or by increasing the Bragg angle by using a beam of smaller energy, as long as the energy is sufficient to obtain a high-momentum transfer peak [(16 0 0)] and has an absorption depth greater than the path length through the stack of dies.

The 2.5%–3% variation in intensity seems to be a systematic error rather than simply due to noise. Currently, we do not understand the cause of this variation. Obtaining a baseline image, which would be generally required for

a 3D integrated circuit which contains devices and wires, may reduce the temperature uncertainty coming from the intensity variation.

Finally, we note that our mapping experiment at Argonne (APS Beamline 1-ID-E) utilizes several desirable properties of a synchrotron source: an x-ray beam with high energy and intensity and a small beam spot size, and these properties are required for a sensitive and accurate temperature mapping. High-energy x-rays are required to obtain diffraction intensities for a high-momentum transfer peak like the (16 0 0) plane. High-momentum transfer is desirable for sensitive thermometry, as the Debye-Waller factor scales as $(1/d)^2$ [12]. An energy of 72 keV, however, is not a requirement to obtain a diffraction peak for the (16 0 0) plane. In fact, any x-ray energy above about 19 keV can satisfy the Bragg condition to obtain a (16 0 0) peak. High photon flux is required to obtain a high enough diffraction intensity for accurate temperature mapping.

Given the requirement for a high enough energy (at least >20 keV), a high incident flux, and preferably small bandwidth, there are two x-ray sources that could make this experiment laboratory sized [30].

The first is a compact Compton source (CCS), which is essentially a laboratory synchrotron source and produces pulsed x-rays [31]. One such commercially available CCS is manufactured by Lycean and produces tunable x-rays with a maximum energy of 35 keV. The Lycean CCS has a photon flux of 10^{10} photons/s with a beam spot size of $100 \times 100\,\mu\text{m}^2$ and an energy bandwidth of 0.3% [32]. The Lycean CCS satisfies all the requirements of an x-ray source to carry out this experiment.

A possibly less expensive and a more traditional lab x-ray source that can be used for the experiment is one using liquid-metal alloys as the anode in the x-ray tube. These x-ray tubes are commercially produced by Excillum and include anodes of metal alloys of indium, silver, or gallium [33]. Of particular interest is the MetalJet E1 model, which, using correct optics, produces indium $K\alpha$ (24 keV), at about 10^8 photons/s with a beam spot size of $90 \times 90\,\mu\text{m}^2$ and a bandwidth of 0.1% [33].

In the kinematic limit, the integrated intensity from a Bragg peak scales as $I \propto I_0(\lambda^3/(\mu \sin 2\theta))$ [12]. For a liquid-anode source (24 keV, $\lambda = 0.52$ Å), for a (16 0 0) peak in silicon, $2\theta \approx 99°$ and $\mu \approx 7$ cm^{-1}. At 72 keV, $\lambda = 0.172$ Å, $2\theta \approx 29.5°$, and $\mu \approx 0.6$ cm^{-1} [11]. Therefore, for the same flux, bandwidth, integration time, and the number of integrated points, the diffraction intensity due to a 24-keV beam is expected to be similar to the diffraction intensity due to a 72-keV beam (a factor of 1.2 higher). The relative bandwidth of the liquid-anode sources is similar to the relative bandwidth used in our experiment at the synchrotron, i.e., $\Delta E/E = 1 \times 10^{-3}$. The flux of a liquid-anode source ($\approx 10^8$ photons/s) is smaller than the flux used in our experiment at the synchrotron (5×10^9 photons/s) by a factor of 50. For the same step size of sample rotation, and the same number of points acquired in the rocking curve, we expect the intensity of the top die to be smaller by a factor of $50/1.2 = 40$. The integrated intensity (for 20-s integration, 10 spots with steps of 0.005°) obtained in the synchrotron for top die is about 80 000 counts per spot, and therefore, using a liquid-anode source, we expect about 2000 counts per spot. The statistical noise due to 2000 counts per spot is $\left(1/\sqrt{2000}\right) \times 100\ \% \approx 2.2\%$ of the signal. Therefore, the expected count is enough to obtain a temperature resolution of 3 K for the top die.

A reduction in the energy of the x-ray beam produced by the liquid-anode metal source compared to a 72-keV beam, however, affects the number of dies in a stack that can be probed. For a stack of four dies and three separators, while the diffraction from the bottom die has an attenuation by a factor of about 3 for a 72-keV beam, the attenuation is about a factor of 35 for a 24-keV beam (see Sec. III of the Supplemental Material [29]). Therefore, while statistical noise from the bottom die is about 4% of the signal using a 72-keV beam, it is about 13% of the signal when using a 24-keV beam. Thus, for a stack of four dies, using a liquid-anode source, the temperature resolution reduces to about 15 K for the fourth die for an integration time of 20 s.

ACKNOWLEDGMENTS

The authors thank Dr. Toby Woods of the School of Chemical Sciences, University of Illinois, for assistance with the experimental setup and data collection for the diffraction experiments. The authors also thank Professor Seok Kim and Dr. Jun Kyu Park of the Department of Mechanical Science and Engineering, University of Illinois, for help with the stacking of silicon dies. This research is funded by the Semiconductor Research Corporation (Task ID 3044.0001). This research uses resources of the Advanced Photon Source, a U.S. Department of Energy (DOE) Office of Science User Facility operated for the DOE Office of Science by Argonne National Laboratory under Contract No. DE-AC02-06CH11357.

[1] A. N. Nowroz, R. Cochran, and S. Reda, in *DAC'10: Proceedings of the 47th Design Automation Conference* (Association for Computing Machinery, New York, NY, 2010), p. 56.

[2] H. F. Hamann, A. Weger, J. A. Lacey, Z. Hu, P. Bose, E. Cohen, and J. Wakil, Hotspot-limited microprocessors: Direct temperature and power distribution measurements, IEEE J. Solid-State Circuits **42**, 56 (2007).

[3] A. Majumdar, Scanning thermal microscopy, Annu. Rev. Mater. Sci. **29**, 505 (1999).

[4] J. Als-Nielsen and D. McMorrow, *Elements of Modern X-Ray Physics* (Wiley, London, 2011).

[5] H. H. Li, Refractive index of silicon and germanium and its wavelength and temperature derivatives, J. Chem. Phys. Ref. Data **9**, 561 (1980).

[6] F. Lu, I. Bhattacharya, H. Sun, T.-T. D. Tran, K. W. Ng, G. N. Malheiros-Silveira, and C. Chang-Hasnain, Nanopillar quantum well lasers directly grown on silicon and emitting at silicon-transparent wavelengths, Optica **4**, 717 (2017).

[7] A. Shakouri, A. Ziabari, D. Kendig, J. H. Bahk, Y. Xuan, P. D. Ye, K. Yazawa, and A. Shakouri, in *2016 32nd Thermal Measurement, Modeling & Management Symposium (SEMI-THERM)* (IEEE, San Jose, CA, 2016), p. 128.

[8] I. Y. Yanina, A. P. Popov, A. V. Bykov, I. V. Meglinski, and V. V. Tuchin, Monitoring of temperature-mediated phase transitions of adipose tissue by combined optical coherence tomography and Abbe refractometry, J. Biomed. Opt. **23**, 1 (2018).

[9] P. B. Johnson and R. W. Christy, Optical constant of the noble metals, Phys. Rev. B **6**, 4370 (1972).

[10] K. D. Cummings, J. C. Garland, and D. B. Tanner, Optical properties of a small-particle composite, Phys. Rev. B **30**, 4170 (1984).

[11] J. H. Hubbell and S. M. Seltzer, *X-Ray Mass Attenuation Coefficients*, https://www.nist.gov/pml/x-ray-mass-attenuation-coefficients (2009).

[12] B. E. Warren, *X-Ray Diffraction* (Dover, 1968).

[13] V. Arp, J. H. Wilson, L. Winrich, and P. Sikora, Thermal expansion of some engineering materials from 20 to 293 K, Cryogenics **2**, 230 (1962).

[14] P. Jiang, X. Qian, and R. Yang, Time-domain thermoreflectance (TDTR) measurements of anisotropic thermal conductivity using a variable spot size approach, Rev. Sci. Instrum. **88**, 1 (2017).

[15] D. M. Hamby, A review of techniques for parameter sensitivity, Environ. Monit. Assess. **32**, 135 (1994).

[16] H. Watanabe, N. Yamada, and M. Okaji, Linear thermal expansion coefficient of silicon from 293 to 1000 K, Int. J. Thermophys. **25**, 221 (2004).

[17] C. Flensburg and R. F. Stewart, Lattice dynamical Debye-Waller factor for silicon, Phys. Rev. B **60**, 284 (1999).

[18] G. Wehmeyer, K. C. Bustillo, A. M. Minor, and C. Dames, Measuring temperature-dependent thermal diffuse scattering using scanning transmission electron microscopy, Appl. Phys. Lett. **113**, 1 (2018).

[19] A. Guinier, *X-Ray Diffraction in Crystals, Imperfect Crystals, and Amorphous Bodies* (W.H. Freeman and Comapny, San Francisco, 1963).

[20] B. W. Batterman, Effect of thermal vibrations on diffraction from perfect crystals, Phys. Rev. **127**, 686 (1962).

[21] B. W. Batterman and D. R. Chipman, Vibrational amplitudes in germanium and silicon, Phys. Rev. **127**, 690 (1962).

[22] K. Kohra, S. Kikuta, S. Annaka, and S. Nakano, Study on temperature effect on x-ray diffraction curves from single crystals by a triple-crystal spectrometer, J. Phys. Soc. Jpn. **21**, 1565 (1966).

[23] K. Kohra, S. Kikuta, and S. Annaka, Temperature effect on the profile of x-ray diffraction of the Bragg case from a germanium single crystal, J. Phys. Soc. Jpn. **20**, 1964 (1965).

[24] P. J. Brown, A. G. Fox, E. N. Maslen, M. A. O'Keefe, and B. T. M. Willis, in *International Tables for Crystallography* (2006), Vol. C, p. 554.

[25] J. Will, A. Gröschel, D. Kot, M. A. Schubert, C. Bergmann, H. G. Steinrück, G. Kissinger, and A. Magerl, Oxygen diffusivity in silicon derived from dynamical x-ray diffraction, J. Appl. Phys. **113**, 1 (2013).

[26] C. Michaelsen, P. Ricardo, D. Anders, M. Schuster, J. Schilling, and H. Gobel, Improved graded mirrors for XRD applications, Adv. X-Ray Anal. **42**, 308 (2000).

[27] E. B. Knudsen, H. O. Sørensen, J. P. Wright, G. Goret, and J. Kieffer, FabIO: Easy access to two-dimensional x-ray detector images in PYTHON, J. Appl. Crystallogr. **46**, 537 (2013).

[28] S. D. Shastri, K. Fezzaa, A. Mashayekhi, W. K. Lee, P. B. Fernandez, and P. L. Lee, Cryogenically cooled bent double-Laue monochromator for high-energy undulator x-rays (50–200 KeV), J. Synchrotron Radiat. **9**, 317 (2002).

[29] See the Supplemental Material at http://link.aps.org/supplemental/10.1103/PhysRevApplied.18.014076 for estimated heating due to incident x-ray flux, calculation of the separation of diffracted beams from two dies, and a comparison of expected diffraction intensities using 72- and 24-keV beams, which also includes Refs. [34–36].

[30] S. Bartzsch and U. Oelfke, Line focus x-ray tubes—a new concept to produce high brilliance x-rays, Phys. Med. Biol. **62**, 8600 (2017).

[31] M. Jacquet, High intensity compact Compton x-ray sources: Challenges and potential of applications, Nucl. Instrum. Methods Phys. Res., Sect. B **331**, 1 (2014).

[32] B. Hornberger, J. Kasahara, M. Gifford, R. Ruth, and R. Loewen, A compact light source providing high-flux, quasi-monochromatic, tunable x-rays in the laboratory, Proc. SPIE **1111003**, 2 (2019).

[33] D. H. Larsson, P. A. C. Takman, U. Lundström, A. Burvall, and H. M. Hertz, A 24 keV liquid-metal-jet x-ray source for biomedical applications, Rev. Sci. Instrum. **82**, 1 (2011).

[34] C. J. Glassbrenner and G. A. Slack, Thermal conductivity of silicon and germanium from 3 K to the melting point, Phys. Rev. **134**, A1058 (1964).

[35] C. T. Anderson, The heat capacity of silicon at low temperatures, J. Am. Chem. Soc. **52**, 2301 (1930).

[36] D. G. Cahill, Thermal conductivity measurement from 30 to 750 K: The 3ω method, Rev. Sci. Instrum. **61**, 802 (1990).